1 **Electronic Supplementary Information**

2

3 **Bio-inspired, Sensitivity-enhanced, Bi-directional Airflow Sensor**

4 **for Turbulence Detection**

5

6 **Fu Liu[a], Yufeng Zhao[a], Nan Xie[a], Yueqiao Wang[a], Meihe Liu[a], Zhiwu Han[b], Tao**
7 **Hou[a*]**

8

9 a. *College of Communication Engineering, Jilin University, Changchun 130022, China*

10 b. *Key Laboratory of Bionic Engineering, Jilin University, Changchun 130022, China*
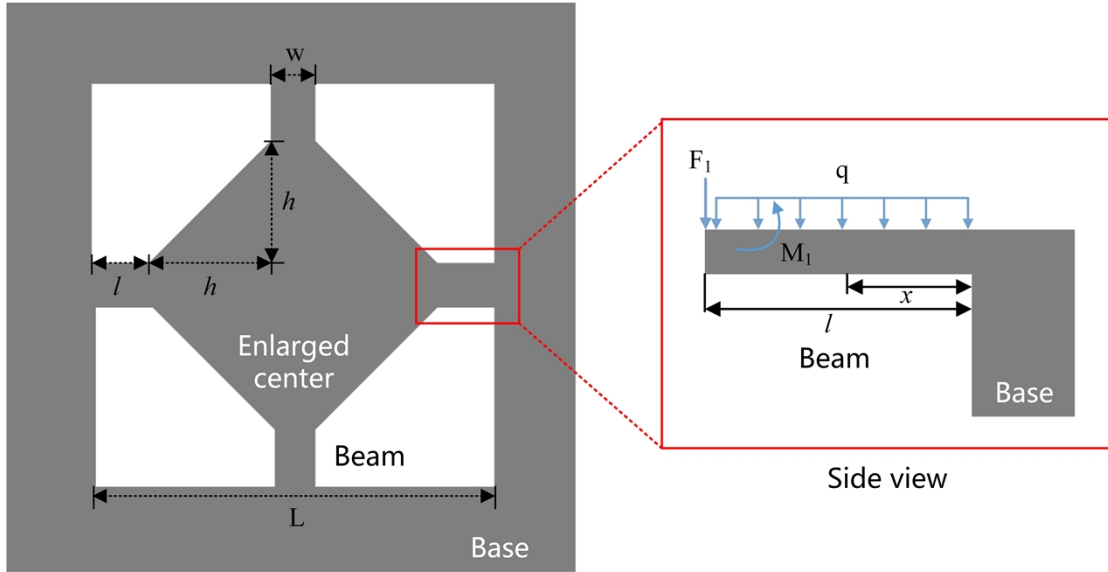
11

_____

12 ***Corresponding author:** Tao Hou

13 **E-mail:** ht_happy@jlu.edu.cn

14

15

1 **Supporting information S1:**

2

3

4 **Figure S1.** The geometrical dimensions of the cruciform beam with an enlarged center,

5 and the side view of the beam under airflow pressure.

6

7 The external stimulus such as wind pressure led to beam deflection and induced stress

8 inside the beam. To analyze the effect of the enlarged center of the cruciform beam, we

9 built a theoretical model of the cruciform beam with an enlarged center under the flow

10 field. The parameters of the cruciform beam with an enlarged center are shown on the

11 left of Fig. S1. The center of the cruciform is enlarged by complementing the center

12 corners with isosceles right triangles. The relationship between the length of the center

13 opening L, the width of the cruciform beam w, the length of the right-angled side of

14 central right triangles h, and the length of the beam l satisfies equation 1:

15
$$L = w + 2 * (l + h) \tag{1}$$

16 When air flows through the cruciform beam from the front, the schematic diagram

17 of the forces on the beams is shown on the right of Fig. S1. Three loads appear on the

18 beam: the wind pressure q applied on the beam, force F_1 produced by the enlarged

19 center under wind pressure and averaged by four beams, and torque M_1 caused by the

20 bending deformation of the enlarged center. The force F_1, which relates to the area of

2

the enlarged center, can be calculated by averaging the total force with four beams as equation 2:

$$F_1 = \frac{1}{4}q(2h^2 + 4hw + w^2)$$

(2)

The torque M_l on the beam at the position x away from the base can be defined as equation 3:

$$M_l = M_1 - F_1(l - x) - \frac{qw(l - x)^2}{2}$$

(3)

The bending angle θ_l caused by the torque at position x on the beam can be obtained by integrating the torque as equation 4:

$$\theta_l(x) = \int_0^x \frac{M_l(x)}{E_b I_{bz}} dx + C$$

(4)

Where, E_b is the elastic modulus of the beam, and C is a constant. I_{bz} is the moment of inertias of the beam along the Z direction, and is defined as equation 5:

$$I_{bz} = \frac{1}{12}wt^3$$

(5)

Where t is the thickness of the beam. The deflection of the beam W_l at the position x on the beam can be calculated by integrating the bending angle as equation 6:

$$W_l(x) = \int_0^x \theta_l(x) dx + Cx + D$$

(6)

Where D is a constant. The values of C and D can be obtained by plugging the boundary conditions into the formula. When the value of x is zero, which is the joint of the beam and base, the values of the bending angle θ_l and deflection of the beam W_l are zero. Thus, the constants C and D are both 0. When considering the position of the end of the beam, the bending angle θ_l is zero. Then we get the torque M_1 as demonstrated in equation 7:

$$M_1 = \frac{1}{24}(6qlh^2 + 3qlw^2 + 4qwl^2 + 12qlhw)$$

(7)

3

1 The deflection of the beam W_l can be obtained when substituting M_1 into the equations

2 and shown in equation 8:

$$M_l(x) = \frac{1}{24}\left(\begin{array}{c} -12qwx^2 + 12qh^2x + 24qhwx + 6qw^2x \\ + 24qlwx - 6qlh^2 - 12qlhw - 3qlw^2 - 8qwl^2 \end{array}\right) \tag{8}$$

3

4 The longitudinal stress δ_l can be determined by equation 9:

$$\delta_l = -\frac{M_l(x)}{W} \tag{9}$$

5

6 Where W_z is the section modulus in Z direction bending and shown in equation 10:

$$W_z = \frac{1}{6}wt^2 \tag{10}$$

7

8 Then the longitudinal stress δ_l can be calculated by equation 11:

$$\delta_l = \frac{1}{4wt^2}\left[\begin{array}{c} 12qwx^2 - (12qh^2 + 6qw^2 + 24qhw + 24qlw)x \\ + 6qlh^2 + 3qlw^2 + 8qwl^2 + 12qlhw \end{array}\right] \tag{11}$$

9

10 When the air flows from the back of the cruciform beam, the direction of the stress and

11 bending angle are reversed without changing the calculation method.

12

13

1 **Supporting information S2:**

2

3 **Table S1.** The geometrical parameters of the cruciform beam with the enlarged center.
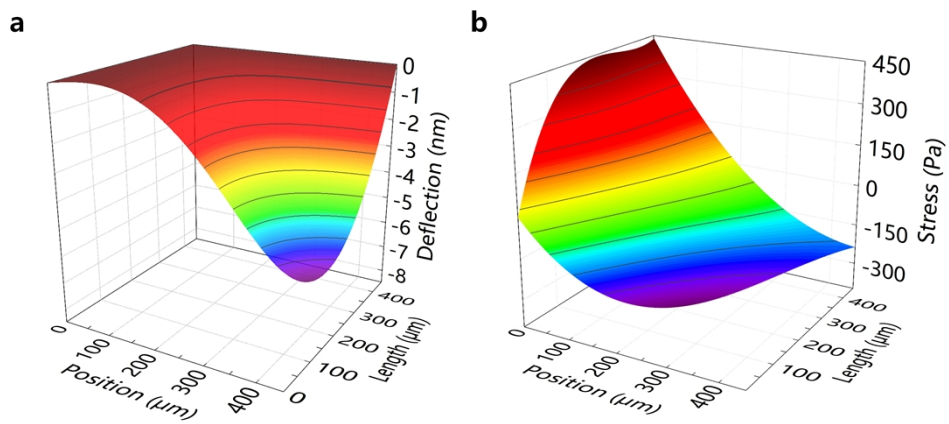
Parameters of the cruciform beam with enlarged center	Parameters
Length of the center opening (L)	1000 μm
Width of the cruciform beam (W)	100 μm
The thickness of the cruciform beam (t)	50 μm
Width of the base	500 μm
Length of the base	1000 μm
Thickness of the base	450 μm
Poisson's ratio	0.23
Young's modulus	160 GPa
Wind pressure	2.5 Pa

4

5

Supporting information S3:

Figure S2. The analysis results of deflection and stress on the whole beam based on the theoretical models when increasing the length of the beam.

The external stimulus of airflow pressure led to the surface stress variation and produced the cruciform beam deflection. We focused on the beam with a concentration of stress and larger deformation due to the smaller width compared to the enlarged center. The deflection and stress results based on the theoretical model are shown in Fig. S2. According to the deflection results, the closer the position of the beam is to the center, the larger the deflection. The maximum deflection increases and decreases with the increase of the beam length. This is because the longer the beam, the smaller the center size and diminished force applied to the cruciform beam. As for the stress results, the root of the beam is subjected to tensile force with a stress value greater than 0, and the joint part to the center is subjected to compressive force. The extreme values of stress appear at the ends of the beam where at the intersection with the base and center. The maximum stress of 443.8 Pa and minimum stress of -392.65 Pa appear at the root and end of the beam when the length is 255 and 206 μm, respectively.

Supporting information S4:

The effects of CTS on the center enlarged cruciform beam were analyzed using fluid-solid coupling models in finite element analysis (FEA) software (ANSYS Workbench 2019). The cruciform beam in this analysis was made of silicon material with Young's modulus of 160 GPa and Poisson's ratio of 0.23. It was positioned in the center of a square tube of $6\times6\times6$ m^3 in size. Flowing air at 2 m/s speed entered the tube inlet while the pressure at the tube outlet was maintained at 0 Pa. The density, viscosity, and temperature of the air were set to 1.225 Kg/m^3, 1.7894×10^{-5} Kg/m·s, and 288.16 K, respectively. The structural element was SOLID186. The bi-directional performance of the cruciform beam was analyzed by turning it over under a consistent airflow direction.

1 **Supporting information S5:**

2
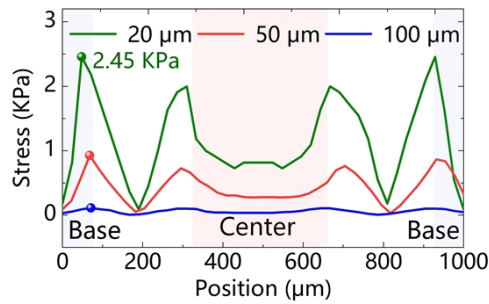
3

4 **Figure S3.** The stress distribution on the bioinspired center enlarged cruciform with

5 various thicknesses (20, 50, and 100 µm).

6   The stress distribution on the bioinspired center enlarged cruciform with various

7 thicknesses (20, 50, and 100 µm) under the same pressure of 2.5 Pa is shown in Fig.

8 S3. The results revealed that the stress on the beam is concentrated in the areas where

9 the beam meets the center and base. As the beam thickness is reduced, the maximum

10 stress rises from 0.09 to 2.45 KPa. The improved maximum stress value implies an

11 increased sensitivity of the sensor, but the overly concentrated stress results in a high

12 fracture risk which reduces the durability. Therefore, to balance the sensitivity and

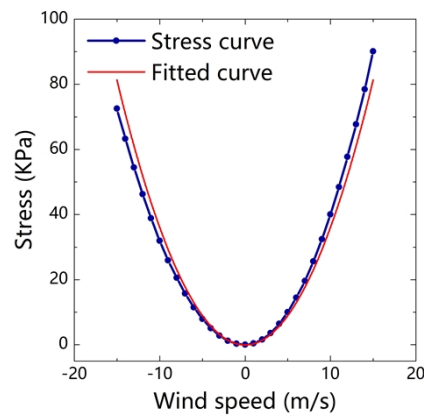13 durability, we determined the thickness of the beam to be 50 µm.

14

15

16

Supporting information S6:

2

3

4 **Figure S4.** The maximum stress on the cruciform beam with CTS and enlarged center

5 when increasing the airflow speed from 0 to ±15 m/s by FEA analysis.

6

7 To investigate the response of the cruciform beam with CTS and enlarged center

8 detecting bi-directional stimuli, we increased the airflow speed from 0 to ±15 m/s of

9 the FEA analysis. The maximum stress, which reflects the distribution of load, on the

10 structure was collected as shown in Fig. S4. The maximum stress values are highly

11 fitted to an asymmetry curve with the R^2 of 0.97495, and the equation of the fitted curve
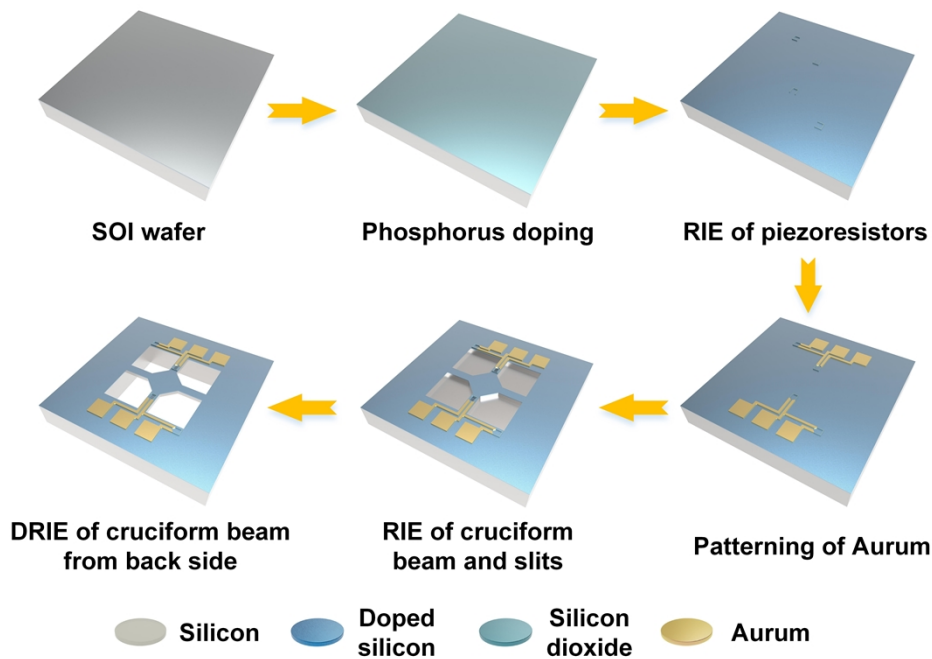
12 is described in equation 12:

13
$$Y = 0.36148x^2 - 0.04482 \tag{12}$$

14

15

9

2

3

4   **Figure S5.** The fabrication process of BSBA.

5

6   The proposed BSBA was fabricated using a MEMS manufacturing process as shown

7   in Fig. S5. A p-type Silicon-On-Insulator (SOI) wafer with a device Si layer thickness

8   of 0.3 μm, an isolation SiO_2 layer of 1 μm, and a handle Si layer of 450 μm was selected

9   as the substrate. The top device layer was doped with n-type phosphorus and thermally

10 annealed for activation. The piezoresistor was etched into a U-shaped pattern with a

11 sheet resistance of 300 Ω per square. Next, aurum thin film with a thickness of 0.5 μm

12 was sputtered and patterned to create wires connected to the piezoresistors completing

13 a circuit. The enlarged center and CTS structures were fabricated by etching the device

14 layer and isolation layer to a depth of 50 μm with a reactive ion etching (RIE) process.

15 Finally, the cruciform beam was released by etching the handle layer from the backside.

16 The completed beam was 100 μm in width and 50 μm thick. Six slits with circular tips

17 were divided into two groups and distributed along one beam on the joint of the beam

18 and center. Two piezoresistors were positioned around each slit to detect the

10

deformation of the beam, with another two piezoresistors distributed on the base. The four piezoresistors formed a Wheatstone bridge configuration. The Wheatstone bridge was powered by a 5V DC supply, and voltage change in the circuit indicated the deformation of the cruciform beam. To enable BSBA to detect bi-directional airflow, a hole with a diameter of 1 mm was carved at the corresponding position on the PCB board.
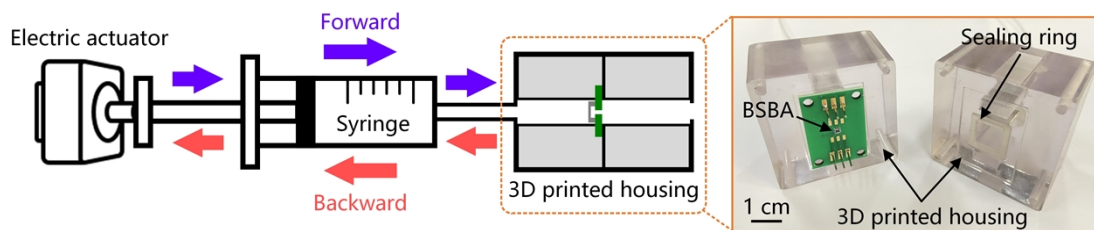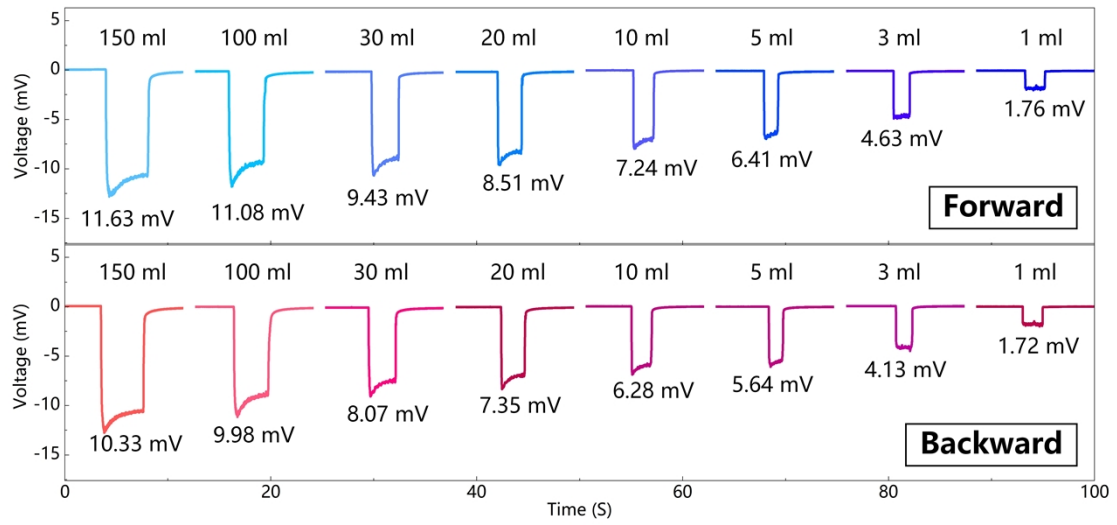
Supporting information S8:

Figure S6. Illumination of BSBA detecting different airflow volumes.

1 **Supporting information S9:**

2

3

4 **Figure S7.** BSBA detecting eight decreasing airflow volumes of 150 ml to 1 ml from

5 forward and backward.
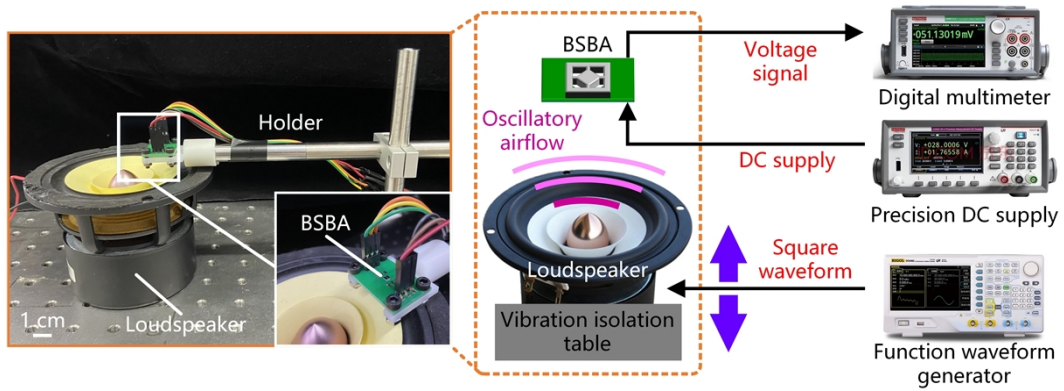
1 **Supporting information S10:**

2

3 **Table S2.** The performance comparison of BSBA with other MEMS piezoresistive

4 flow sensors.

Sensing unit	Quantity	Sensitivity	Sensing range	Response time	Bi-directional capability
Microcantilever with an enlarged free end[1]	1	0.0284 Ω/m/s	0-45 m/s	530 ms	No
Microcantilever with a corrugated structure[2]	1	1.157×10^{-2} /m/s (ΔR/R)	0.2-1 m/s	3.72 s	No
Microcantilever with focused-ion-beam[3]	1	3.22×10^{-5} /m/s (ΔR/R)	0-4 m/s	No data	No
Microcantilever[4]	1	5.5×10^{-4} /m/s (ΔR/R)	2-20 m/s	No data	No
Curved microcantilevers[5]	2	40 μV/m/s (±10-20 m/s) 80 μV/m/s (±20-32 m/s);	±10-32 m/s	No data	Yes
Curved microcantilevers[6]	4	60.35 mV/m/s (≥38.5m/s)	0-±40.5 m/s	No data	Yes
BSBA (this study)	1	**1.36** mV/m/s (0-±2m/s) **0.53** mV/m/s (±2-5m/s)	**0-±5 m/s**	**24.1 ms**	**Yes**

5

Supporting information S11:

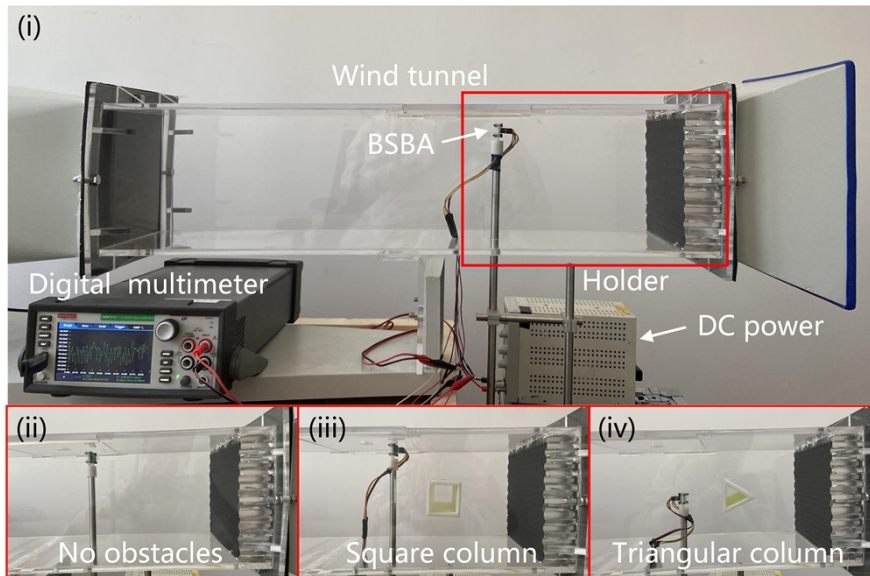**Figure S8.** Illustration of BSBA detecting oscillatory airflow produced by a

loudspeaker.

Supporting information S12:
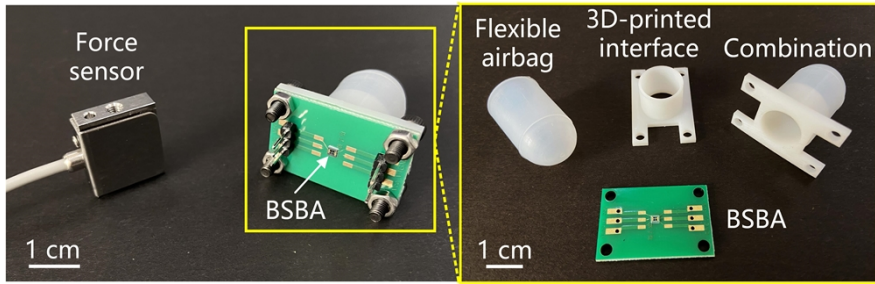
Figure S9. Images of BSBA detecting flow field change caused by the square column

and triangular column compared to without obstacles within the wind tunnel.

Supporting information S13:

Figure S10. The images of the force sensing module of the BSBA.

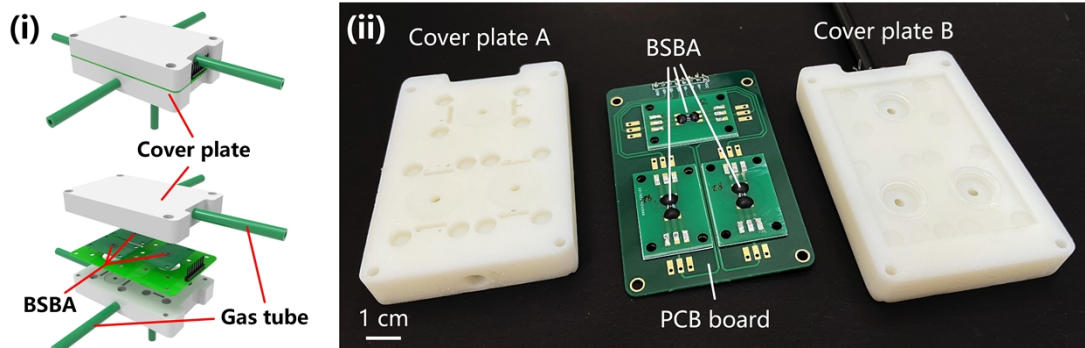**Supporting information S14:**

Figure S11. The components of the BSBA sensor package.

Supporting information S15:

The obstacle detection system consists of three parts: the quadrotor, sensor package, and software. The 370×370×240 mm^3 quadrotor (DJI F450) was securely mounted on the platform to prevent any unintended movement. The quadrotor was equipped with 9450 self-locking propellers actuated by 2312KV800 brushless motors which generated downwash airflow. The presence of an approaching obstacle affects the flow field around the quadrotor; these variations were detected by the sensor package attached to the bottom of the quadrotor's center. The sensor package consists of three BSBA sensors attached on a PCB board by soldering, 3D printed housing with internal air paths 3 mm in diameter, and 35 cm PVC tubes of 3 mm inner diameter and 6 mm outer diameter connecting the sensor to the quadrotor. The up and down tubes were made from flexible hoses and the front, back, left, and right tubes were rigid. The flow field information captured by BSBA was transmitted to the computer via a multichannel wireless data acquisition module (VKinging Electronics, VK701W, China) using a Wi-Fi communication link. The sampling frequency of the acquisition module is 480 Hz. The obstacle detection software processed the received flow field information and determined the position of the detected obstacle.

1 **Supporting information S16:**

2
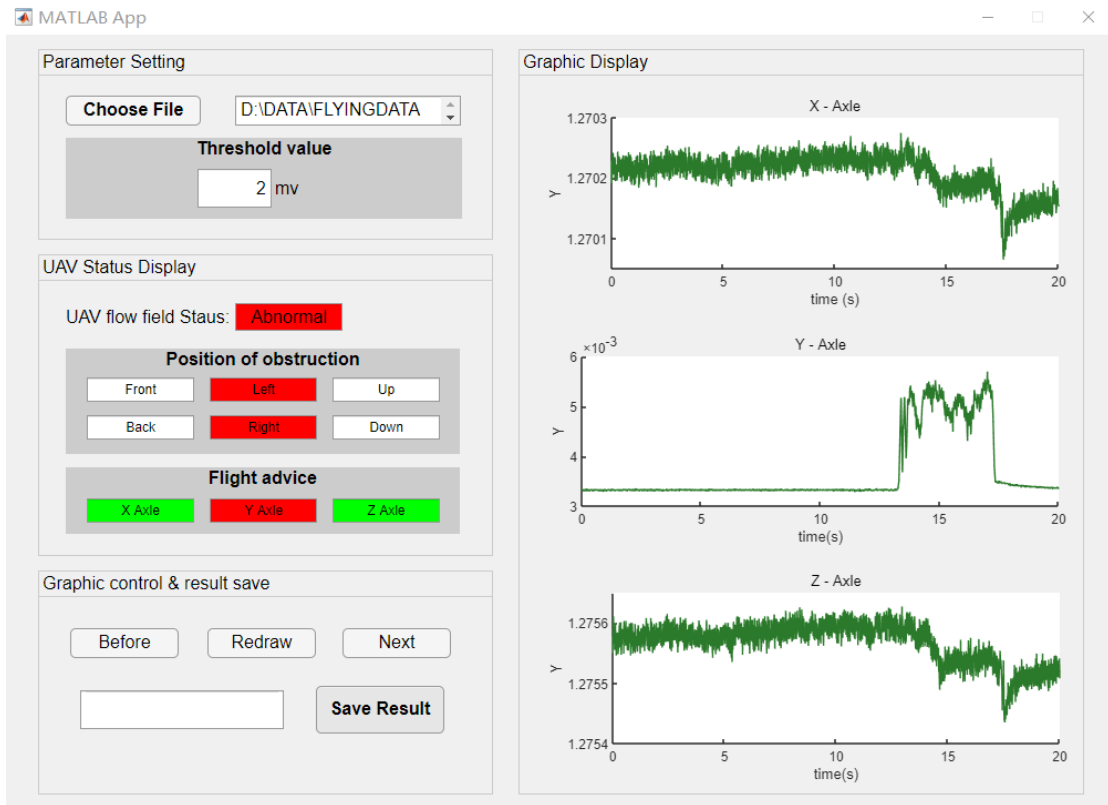
4 **Figure S12.** The operation interface of quadrotor-based obstacle detection software.

5

6

References

1 Y. H. Wang, C. Y. Lee and C. M. Chiang, *Sensors*, 2007, **7**, 2389–2401.

2 D. K. Choi and S. H. Lee, *Microelectron. Eng.*, 2012, **98**, 477–482.

3 D. K. Choi and S. H. Lee, *Integr. Ferroelectr.*, 2014, **157**, 157–167.

4 H. Takahashi, A. Nakai and I. Shimoyama, *Sensors Actuators, A Phys.*, 2018, **281**, 243–249.

5 C. Abels, A. Qualtieri, T. Lober, A. Mariotti, L. D. Chambers, M. De Vittorio, W. M. Megill and F. Rizzi, *Beilstein J. Nanotechnol.*, 2019, **10**, 32–46.

6 D. Shen, Y. Jiang, Z. Ma, P. Zhao, Z. Gong, Z. Dong and D. Zhang, *J. Bionic Eng.*, 2022, **19**, 73–82.